

Achilles: a search for Trojans in the Earth-Moon system

Author: Iris Ortega Casas.

Facultat de Física, Universitat de Barcelona, Diagonal 645, 08028 Barcelona, Spain.

Advisor: Jorge Núñez de Murga

Abstract: Several Trojans have been found in the Solar System, but no Earth-Moon Trojans (EM-Ts) have been discovered yet. There have only been two surveys for EM-Ts, by Valdes & Freitas [1](1983) and Gregg & Wiegert [2](2022), both centered around L4 & L5. In this work we introduce a new pipeline for EM-Ts based on the theoretical frame developed by Jorba [3–5], which shows that they may be found at some distance from L4 & L5. More specifically, this work focuses on the development of **Achilles**, an automated asteroid detection tool. We have successfully validated it by detecting Main Belt Objects. However, we have applied it on some of our EM-T images and found no EM-Ts. Even so, this new tool will ease the process towards their possible discovery.

I. INTRODUCTION

The three-body problem (TBP) consists of a chaotic system of three bodies, each disturbed by the gravitational field of the other two. To solve it we require mathematical approximations such as the restricted TBP[4]. This model supposes that two of the bodies are much bigger than the third one (i.e., its mass is negligible), that those two have circular orbits around their center of mass, and that the bodies are point masses. In such case, there exist five equilibrium points, called Lagrangian points and labeled LP (with P being 1, 2, 3, 4 or 5). While three of these points are not stable, two of them, L4 and L5, are. Therefore, the two last ones are a good place for finding asteroids as they will remain there for prolonged periods of time. A more realistic model is the Bicircular Problem (BCP)[4], which adds the effects of the Sun’s gravity on the system, making the original two bigger bodies revolve in a circular orbit around the Sun. All bodies in the BCP are considered coplanar.

L4 and L5 are located at the vertices of each equilateral triangle formed by the two larger bodies and the third one; L4 to the left of the most massive body and L5 to the right. Celestial bodies in a stable orbit around L4 and L5 are called Trojans and they may provide us with information about the formation of the Solar System.

In 1906, the first Trojan (588 Achilles) [6] was discovered in the Jupiter-Sun system, validating Lagrange’s theory. Since then, further Trojans have been found in all planet-Sun systems (except for Mercury and Saturn) and even in the systems formed by Saturn and a larger moon (like Polydeuces [7] at Dione’s L5). For the Earth-Sun system only two Trojans have recently been discovered: 2010 TK₇ [8] and 2020 XL₅ [6].

Trojan asteroids in the Earth-Moon (EM) system are yet to be found. Forty years ago a search was made by Valdes & Freitas [1] around all five LPs in the EM system, with a limiting magnitude of 17-19 for L4/L5. However, no Trojan was found probably due to the research being manual, using plates and microscopes [2]. The current technological advances may improve our chances of finding EM Trojans (EM-Ts) nowadays.

Other surveys currently operating (such as CSS [9], ATLAS [10] or Pan-STARRS [11]) deal with objects at slower velocities (MBOs, NEOs, PHAs, etc.)¹ and are not adjusted to the orbits of the hypothetical EM-Ts [2].

Since the Valdes & Freitas [1] search for EM-Ts, there has only been another one, conducted by Gregg & Wiegert [2]. It used four small telescopes with a limiting magnitude ranging from 15.8 to 16.5 for an exposure time of 30 seconds and maximum FoV of $3.98^\circ \times 3.98^\circ$. Their observations were centered on L4 & L5.

Our EM-T search method has been developed using the theoretical framework published in [3–5], based on the BCP and including the effects of adding the other planets to the system, which show that the EM-Ts remain in orbit around L4 and L5 for at least 1000 years. Our survey uses the TFRM (Telescopi Fabra-ROA al Montsec) [12], with a FoV of $4.4^\circ \times 4.4^\circ$ and a limiting magnitude of around 17.5 for 30 seconds frames. These features make the TFRM an excellent tool to find new EM-Ts thanks to its big FoV, its fast tracking speed, and its capability of detecting fainter objects. Observations began the last semester of 2021 and are still ongoing.

The present work discusses the chosen strategies for our survey (Section II) and focuses on the selection, filtering, and processing of the images obtained (Sec. III), the development of **Achilles**, an automated asteroid detection software, using Main Belt (MB) images to test it out (Sec. IV) and the attempt to detect EM-Ts using this program (Sec. V). We finish with a discussion of the results and future work (Sec. VI).

II. SURVEY

In the simulations done in [4], the highest survival rate over a thousand years for EM-Ts is for apparent vertical speeds around 0.56 or 0.80 km s⁻¹ (dimensionless values considering the EM distance as 1: $\dot{z} = 0.58$ or 0.83) when

¹ Main Belt Objects, Near-Earth Objects and Potentially Hazardous Asteroids.

crossing the EM plane (see Fig. 1). Since the movement in the vertical direction is similar to that of a harmonic oscillator, the vertical velocities will decrease as the EM-Ts get farther from the LPs. Therefore we may improve our chances of finding EM-Ts if we search around the region where they are the farthest from the EM plane, as their vertical velocity would be virtually null. Since the dimensionless speed when crossing the EM plane is equivalent to that maximum distance, we can find the angles where the EM-Ts would have $\dot{z} \approx 0$ by computing $\arctan(\dot{z})$, which gives us an approximate range of 30° to 40° [3]. Still, to take into account other studies and the tiny population around $\dot{z} = 0.35$, we have amplified the range from 14° to 41.2° , only above the LP since the ones under it are more difficult to observe from the TFRM.

For our survey, we have vertically divided this region into 7 fields, which overlap 0.6° . We take 5 images, spaced 32 s (to take into account readout, moving, and tracking time) of each field with a 30 s exposure time. To obtain an optimal number of images each night, we have developed two strategies:

1. A mosaic ($1 \times 7 \times 5$) formed by one column with 7 fields, taking 5 images for each field before moving to the next one. It requires 2138 s (which means EM-Ts would move ~ 300 pixels) and provides us with a total field of $4.4^\circ \times 27.2^\circ$.
2. A mosaic ($2 \times 7 \times 5$) formed by two columns with 7 fields (overlapping 0.6° horizontally), taking an image for each field in a row in turns until reaching 5 for each one before moving to the next row. It requires 4308 s (EM-Ts would move ~ 600 pixels) and provides us with a total field of $8.2^\circ \times 27.2^\circ$.

By alternating these strategies and, using only the first one when the LPs are not visible for a long period of time, we can obtain hundreds of images on a clear night.

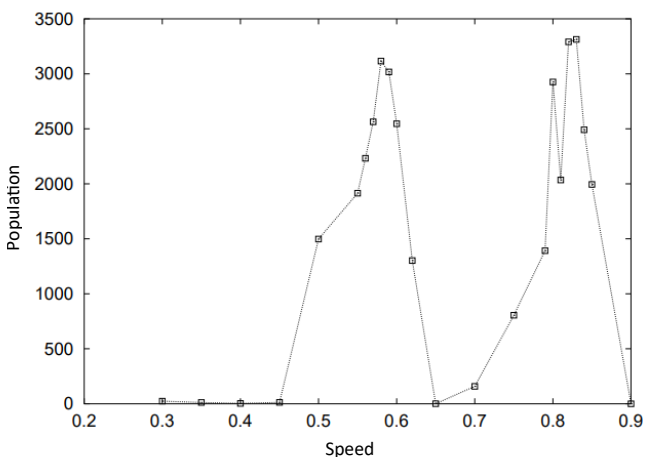


FIG. 1: Extracted from [4]. Vertical axis: estimate of the EM-T population in the stability region that survives a thousand years without escaping. Horizontal axis: the dimensionless speed of the EM-Ts when crossing the EM plane.

III. IMAGE PROCESSING

To work with the FITS files obtained with the TFRM, from this section onward, we have mainly used the `astropy`² Python library. First of all, we select the EM-T images and their darks³ and flats⁴. Then we filter the images to obtain those with good enough weather conditions and to avoid processing images with the shutter closed or other errors. We keep those images with a temperature of the CCD between -21 & -19 °C and median between 1100 & 20000 and considering other parameters of the characteristics of the TFRM such as the blind being closed.

Once we have our images selected we correct them using the selected flat and dark files. To do so, a masterfile is generated for both types of correction images by stacking the arrays of data of the images and computing the mean value for each pixel. First, a masterdark is generated for each night. Then the flat files are calibrated by subtracting their corresponding masterdark to each one, pixel by pixel, and the masterflat is generated. The scientific images are then corrected by subtracting the masterdark and the normalized masterflat.

Due to the big FoV of the TFRM and its condition as a remotely controlled telescope, flats can not be done every night, therefore we have used the same masterflat for the analysis done in this work. Since our research depends on the coordinates of the detected objects and not their photometry, this does not affect it much.

Finally, the images must be astrometrically reduced, i.e. each pixel in the image must be associated with its corresponding physical coordinates. To do so, we use `Astrometry.net`⁵ and `SExtractor`⁶ by calling them with a custom-made Python wrapper (`sewpy`⁷) and our own-made code. `SExtractor` detects some of the objects in the image and generates a catalog with them, allowing the modification of parameters such as the minimum number of pixels for it to be considered an object, etc. These catalogs are in turn used by `Astrometry.net` to compare with its internal indexes and return the image's coordinates.

IV. ACHILLES: ASTEROID DETECTION SOFTWARE

To process the hundreds of obtained images we have developed a Python-based program to automate the de-

² <http://www.astropy.org>

³ Images taken with the same exposure times as the EM-Ts ones but with the shutter closed such that it only takes into account the dark current due to the noise of each pixel.

⁴ Images taken with uniform lighting such that it takes into account the different quantum efficiency of each pixel, its response to different filters and any imperfection in the optical system (dust, vignetting, etc).

⁵ <https://Astrometry.net>

⁶ <https://www.astromatic.net/software/SExtractor/>

⁷ <https://github.com/megalut/sewpy>

tection of moving objects, as no currently available software completely satisfies our needs. We have named our automated asteroid detection tool **Achilles**.

First, we use **SExtractor** on each image to generate a catalog of detections such that each of the detected objects occupies at least 4 pixels and has a brightness over 1.2 times that of the background. These parameters have been tuned to optimize the detection of the faintest objects in our images.

Then, for each catalog, **Achilles** selects the faintest object, finds its closest match with the Gaia DR3⁸ [13] catalog (using the **astroquery**⁹ package) and saves the corresponding Gaia magnitude. **Achilles** will use this as the limiting magnitude for the image unless it is lower than 18 (since below this number there are not enough matches with the Gaia DR3 catalogs), in which case it will use 18. Then, it loads Gaia DR3 catalogs for each image's region up to the chosen limiting magnitude.

Achilles then proceeds to do three subtractions. First, it matches each image with the corresponding region loaded from Gaia such that the angular distance between matched objects is $< 0.0023^\circ$ (2 pixels). The matched objects are then subtracted from each image's catalog. A similar process is then executed but using each image as a reference for the other images: the 2nd subtraction is done by x, y coordinates to eliminate dead pixels (some may remain even though we constrict **SExtractor** to detections of minimum 4 pixels) and the 3rd one by equatorial coordinates (α, δ) (in case some object has not been matched with the Gaia catalogs but matches with a detection in another image).

The input catalogs are thus reduced from thousands of detections to barely a hundred. Now, each detection is paired with the closest detection (by α, δ coordinates) in each subsequent image. Using these tables of paired detections, **Achilles** builds a table of related detections such that they move a certain maximum velocity between images. It picks each detection on the catalog of the first image and checks that its paired detection in the following image does not surpass the imposed speed. If it does, it keeps checking for its other paired detections on the following images until it finds a correlated detection. This process is done for the ensuing images, always searching for a match in the following images and, if possible, linking the detections to those strings of already built correlated detections.

To ascertain that their movement is approximately linear, we impose that one of the coefficient regressions for each coordinate (α or δ) and time be $R^2 > 0.91$. This method commonly results in less than a hundred possible moving objects.

Finally, in the case of MBOs, using the IMCCE¹⁰

database **Achilles** finds the name of the tabulated asteroids detected. This way we reduce our list of potential candidates to only unknown objects.

A. Problems encountered

While developing **Achilles** we have tested it with a series of MB images to detect problems on the code. The following are the solutions we have proposed:

- **Matching with Gaia catalogs:** choosing the brightness depth of an image to match with the Gaia catalog is difficult. The chosen limiting magnitude might be too faint compared to our image or to a region of it, thus some moving objects detected by **SExtractor** may disappear when matching with a background object from the Gaia catalog.
- **Distance range extrapolation:** to solve the previous problem and to take into account subsequent objects not detected by **SExtractor**, we search for the next detection not only in the next image but in the subsequent images. By doing this, the probability of concatenating a detection in an image with a false positive in a subsequent image increases. Therefore we will have to deal with outliers.
- **Outliers:** to deal with them, first we use a robust median algorithm to find the median value of each set of successive coordinates (right ascension and declination) not contaminated by the outlier. Then, we can extract the outliers via the difference between their coordinates and the robust median values. This way, we can compute the regression coefficient of the array of values for each coordinate, using time as the other axis, not taking into account the outliers. This is a necessary step so as to not eliminate real asteroids due to the outliers decreasing their regression coefficient. However, this step admits strings of detections that are not linearly correlated, therefore this will increment the number of false positives.
- **Regression coefficients:** as some asteroids have significantly small velocities in one coordinate, its error becomes relevant therefore generating a smaller regression coefficient for that coordinate. To counter that, we consider a good set of detections those with $R^2 > 0.91$.
- **Observing conditions:** false positives may also appear due to weather conditions and/or the physical conditions of the telescope. The TFRM telescope presents some scratches on the optical surfaces of the Field-flattener from when it was

⁸ Data Release 3 (2022): <https://www.cosmos.esa.int/web/gaia/data-release-3>

⁹ <https://github.com/astroquery/astroquery>

¹⁰ Institut de mécanique céleste et de calcul des éphémérides:

<https://www.imcce.fr/>.

mounted into the CCD camera by the manufacturer. Therefore these specific regions on the images produce a higher number of detections due to the noise caused by the scratches. However, we do not mask the affected regions as **Achilles** is able to detect asteroids passing through them. Furthermore, if the telescope is not properly collimated or focused, it may induce error in the astrometrical reduction of the images.

- **Blending:** some objects may not be detected when passing in front of or close to a brighter object, which can cause false detections as **Achilles** tries to find the next detection. This can be seen in Fig. 2, where the Gellner asteroid is lost when crossing a brighter object to the right (bottom left image) and **Achilles** concatenates the last detection of Gellner with a false positive. However, thanks to the outlier removal step, this detection has survived the candidate validation process of **Achilles**.

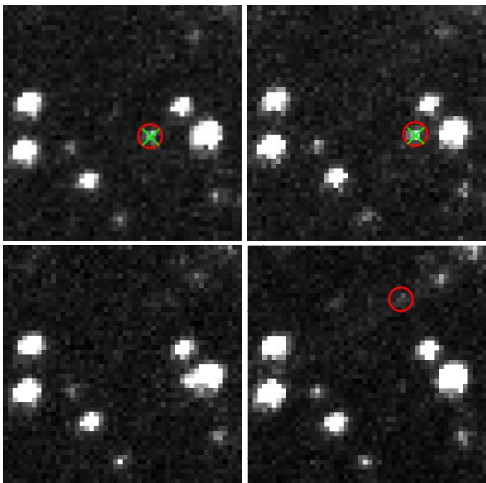


FIG. 2: Images of the Gellner (16.4 mag) asteroid as detected by **Achilles**. The red circle indicates the **Achilles** detections, while the green cross denotes the actual coordinates taken from the IMCCE. It follows a chronological order from left to right and from top to bottom.

B. Tuning parameters

Some parameters of **Achilles** must be tuned to take into account the different types of asteroids/objects one wants to detect and to reduce false positives.

Depending on the type of object to be detected, the speed range must be changed. For MBOs we impose a maximum velocity of 0.022° per hour, which corresponds to a movement of 0.17 pixels in our images of 30 s exposure. On the other hand, EM-Ts move faster. Their horizontal velocity above the LPs is dictated by the movement of these points, which follow that of the Moon (considering the Earth as the point of origin and immobile). Therefore, as the Moon moves at a speed of

$360^\circ/28 \text{ days} \approx 0.54'' \text{ s}^{-1}$, in an image with 30 s of exposure time, EM-Ts may leave a trace of $\sim 16.1''$, which corresponds to ~ 4.2 pixels for our images.

To reduce false positives, the minimum number of detections per string of detections can be changed. For example, when searching for MBOs we have been able to decrease the number of false positives by having an input of 10 or more images and requiring at least 5 detections.

V. RESULTS

In this work, we have developed, tuned and tested **Achilles**, an automated pipeline focused on the detection of asteroids and other moving objects. We have applied it to sets of images from the MB and from our survey for EM-Ts.

A. Main Belt Objects (MBOs)

We have used **Achilles** on three sets of MB images, successfully detecting all corresponding asteroids tabulated on the Minor Planet Center (MPC) up to 17.3 mag.

In Figure 3 we show an example of some of the asteroids detected by **Achilles**: Sahade and Diderot. Sahade is the faintest (17.3 mag) asteroid detected until now by **Achilles**. Diderot is another example of an asteroid not being detected due to passing in front of a brighter object (1st image on its row). It also is an example of almost null velocity in declination, which causes a lower regression coefficient for that coordinate. Our highest detection ratio between actual asteroids and candidates has been of 78%.

We have also compared the coordinates given by the IMCCE and those computed with **Achilles** for some of our detections. The results are shown in the Appendix for two given images, in Tables I and II. We can see that the difference ranges from ~ 0.01 to ~ 1.00 pixels. These errors are within the tolerances of our survey.

B. Earth-Moon Trojans

Thirty nine images from our survey for EM-Ts have been processed using different approaches (processing sets moving horizontally and vertically over the mosaics). As expected, no EM-Ts have been found yet.

One reason for the lack of detections in EM-T images can be found in the study on the stability of the LP regions made by Chambers & Lissauers [14]. This study shows that, while a high population of EM-Ts remains stable for a billion years when considering only solar perturbations, they may be destabilized in a shorter amount of time due to the eccentricities introduced when including the other eight planets in the numerical calculations. Therefore the population of EM-Ts might be small and composed of objects placed there recently in geological timescales, which decreases our probability of finding them.

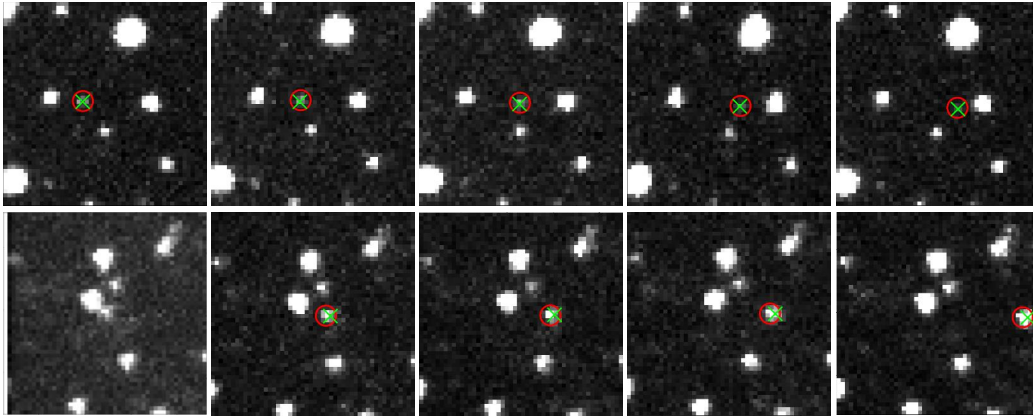


FIG. 3: Examples of MBOs detected by *Achilles*. Again, the red circle indicates the *Achilles* positions while the green cross corresponds to that tabulated on the IMCCE database. The 1st row shows the faintest detected MBO, Sahade, with 17.3 mag. The 2nd row shows Diderot (15.7 mag). It is ordered chronologically from left to right.

However, to check whether *Achilles* could find asteroids using this approach (since the movement between images is greater than for MB images), we have selected some sets close to the ecliptic plane and successfully found its asteroids tabulated in the MPC up to 17.2 mag.

VI. CONCLUSIONS & FUTURE WORK

We have successfully developed *Achilles*, a software for the detection of asteroids by concatenating detections by velocity and linearity. For now, and with the relatively small number of images considered for this work, no EM-Ts have been found. This is to be expected since the previous EM-T surveys, by Valdes & Freitas [1] (1983) and by Gregg & Wiegert [2] (2021) were also unsuccessful. Moreover, the study made by Chambers & Lissauer [14] shows that the probability of finding EM-Ts might be small.

To improve our research, we will study more closely some parameters like the selection of a magnitude to match with the Gaia DR3 catalog and the differentiation of the PSFs (Point Spread Function) of an asteroid and other objects to prevent losing asteroids close to brighter objects. We will also simulate Trojan-like asteroids –of different magnitudes, sizes, speeds and moving

directions– in our images to check whether *Achilles* can actually detect them and modify the program accordingly. Finally, all the images obtained in our survey will be processed with the pipeline developed in this project, and the results checked to have a larger sample.

Still, if no EM-Ts are found, and even so, since we already have more than a hundred nights stored, we could try a different approach to improve our strategies of observation and/or detection.

Furthermore, the camera of the TFRM has recently been changed from a CCD to a more sensitive CMOS camera. Hence, our pipeline will have to be modified accordingly to continue our survey. For example, this means less exposure time to achieve the same limiting magnitude, which changes our strategies or their cadence.

Acknowledgments

This research is framed within the UB-RACAB collaboration grant (2022.2.RACAB.1) and has made use of the Gaia DR3. I want to thank Daniel del Ser, Maite Merino and Jorge Núñez for their help and guidance, as well as the previous grant holders for their work on the preceding steps of this project.

-
- [1] F. Valdes and R. A. Freitas, *Icarus* **53**, 453 (1983).
 - [2] C. R. Gregg and P. A. Wiegert, *MNRAS* **511**, 5396 (2022).
 - [3] À. Jorba, *A & A* pp. 327–338 (2000).
 - [4] À. Jorba, in *Hamiltonian Systems and Celestial Mechanics* (World Scientific, Pátzcuaro, Michoacán, México, 2000), pp. 197–213.
 - [5] M. Jorba-Cuscó, A. Farrés, and À. Jorba, *Frontiers in Applied Mathematics and Statistics* **4**, 32 (2018).
 - [6] T. Santana-Ros et al., *Nature Communications* **13**, 447 (2022).
 - [7] C. C. Porco et al., *Science* **307**, 1226 (2005).
 - [8] M. Connors, P. Wiegert, and C. Veillet, *Nature* **475**, 481 (2011).
 - [9] S. Larson et al., **35**, 36.04 (2003).
 - [10] J. L. Tonry et al., *PASP* **130**, 064505 (2018).
 - [11] N. Kaiser, *Proc. SPIE* **5489** (2004).
 - [12] O. Fors et al., *PASP* **125**, 522 (2013).
 - [13] A. Vallenari et al., arXiv (2022).
 - [14] J. J. Lissauer and J. E. Chambers, *Icarus* **195**, 16 (2008).

Appendix

Name	Right ascension			
	Achilles[°]	IMCCE[°]	Difference [°]	Difference [pixels]
Mali Losinj	253.10295	253.10305	0.00011	0.1
1999 VD68	252.536	252.5365	0.0005	0.4
Frostia	253.6865	253.68647	0.00002	0.02
Pauly	256.8553	256.8541	0.0012	1.1
Handahl	255.0028	255.0021	0.0007	0.7
Tripuraneni	252.66386	252.66379	0.00007	0.07
Diderot	256.9945	256.9929	0.0016	1.5
Spellmann	254.62849	254.62831	0.00019	0.17
Gellner	254.30566	254.30556	0.00010	0.09
Ludekpesek	256.0128	256.0117	0.0010	1.0
1998 KB51	246.4275	246.4266	0.0009	0.8
1999 XY24	246.1698	246.1693	0.0005	0.5
Sahade	244.05888	244.05891	0.00003	0.02

TABLE I: For each asteroid detected in two selected images, it shows the right ascension in degrees as computed using **Astrometry.net** and the one extracted from the IMCCE database. The difference between both values has been computed both in degrees and in pixels for our images.

Name	Declination			
	Achilles[°]	IMCCE[°]	Difference [°]	Difference [pixels]
Mali Losinj	-10.3538	-10.3533	0.0005	0.5
1999 VD68	-11.00975	-11.00978	0.00002	0.02
Frostia	-11.1656	-11.1652	0.0004	0.4
Pauly	-11.71695	-11.71702	0.00007	0.07
Handahl	-11.9166	-11.9162	0.0004	0.3
Tripuraneni	-12.49021	-12.49015	0.00006	0.05
Diderot	-12.48367	-12.48364	0.00003	0.03
Spellmann	-13.5454	-13.545	0.0004	0.4
Gellner	-13.6697	-13.6694	0.0003	0.3
Ludekpesek	-13.45104	-13.45112	0.00008	0.07
1998 KB51	-6.9334	-6.9332	0.0002	0.2
1999 XY24	-8.0084	-8.0077	0.0007	0.7
Sahade	-7.72404	-7.72388	0.00016	0.15

TABLE II: For each asteroid detected in two selected images, it shows the declination in degrees as computed using **Astrometry.net** and the one extracted from the IMCCE database. The difference between both values has been computed both in degrees and in pixels for our images.